Quantification of the effect of site-specific histone acetylation on chromatin remodeling rate

Masatoshi Wakamori[1], Kohki Okabe[2,3,*], Kiyoe Ura[3,4], Takashi Funatsu[2], Masahiro Takinoue[3,5,*], Takashi Umehara[1,3,*]

[1]Laboratory for Epigenetics Drug Discovery, RIKEN Center for Biosystems Dynamics Research, Yokohama, Kanagawa, Japan. [2]Graduate School of Pharmaceutical Sciences, The University of Tokyo, Hongo, Bunkyo-ku, Tokyo. [3]PRESTO, Japan Science and Technology Agency (JST), Kawaguchi, Saitama, Japan. [4]Graduate School of Science, Chiba University. [5]Department of Computer Science, Tokyo Institute of Technology, Yokohama, Kanagawa, Japan.

*Correspondence and requests for materials should be addressed to K.O. (email: okabe@mol.f.u-tokyo.ac.jp), M.T. (email: takinoue@c.titech.ac.jp) or T.U. (email: takashi.umehara@riken.jp).

Abstract

Eukaryotic transcription is epigenetically regulated by chromatin structure and post-translational modifications (PTMs). For example, lysine acetylation in histone H4 is correlated with activation of RNA polymerase I-, II-, and III-driven transcription from chromatin templates, which requires prior chromatin remodeling. However, quantitative understanding of the contribution of particular PTM states to the sequential steps of eukaryotic transcription has been hampered partially because reconstitution of a chromatin template with designed PTMs is difficult. In this study, we reconstituted a di-nucleosome with site-specifically acetylated or unmodified histone H4, which contained two copies of the *Xenopus* somatic 5S rRNA gene with addition of a unique sequence detectable by hybridization-assisted fluorescence correlation spectroscopy. Using a *Xenopus* oocyte nuclear extract, we analyzed the time course of accumulation of nascent 5S rRNA transcripts generated on chromatin templates *in vitro*. Our mathematical model and fitting analyses revealed that tetra-acetylation of histone H4 at K5/K8/K12/K16 increases the chromatin remodeling rate ~3-fold in comparison with the absence of acetylation. We provide a mathematical model for quantitative evaluation of the contribution of epigenetic modifications to chromatin transcription.

Keywords: chromatin, epigenetics, FCS, genetic code expansion, *Xenopus laevis*.

36 Eukaryotic genes are transcribed by three classes of multisubunit DNA-dependent RNA
37 polymerases (RNAPs)[1]. Ribosomal RNA (rRNA) genes, protein-coding genes, and short
38 non-coding genes, including those for 5S rRNA and transfer RNA (tRNA), are transcribed
39 by RNAP I, II, and III, respectively[2-4]. Because eukaryotic genomic DNA interacts with
40 positively charged histone proteins and is compacted into chromatin, gene transcription
41 is regulated not only by processes involving a naked DNA template—such as the
42 recruitment of general transcription factors and RNAPs to the promoter, initiation, and
43 elongation—but also by processes involving a chromatin template, such as chromatin
44 accessibility for the transcription machinery and chromatin remodeling[5,6]. The structural
45 unit of chromatin, the nucleosome, is formed by wrapping DNA (145–147 bp) around
46 the histone octamer, which consists of two copies of each of the core histones (H2A,
47 H2B, H3, and H4)[7,8]. Each core histone has a lysine (K)-rich N-terminal tail that protrudes
48 through nucleosomal DNA, and these lysine residues are subjected to post-translational
49 modifications (PTMs) such as acetylation, methylation, and ubiquitination[9]. Lysine
50 acetylation (Kac) of the histone H4 tail facilitates chromatin transcription by RNAPs I, II,
51 and III in comparison with unmodified histone H4[10-16]; this presumably occurs by
52 enhancing the remodeling or repositioning (or both) of the nucleosome positioned near
53 the transcription start site[17,18].

54 The N-terminal tail of histone H4 has four major acetylation sites (K5, K8, K12, and
55 K16), which are highly conserved from yeast to human. These lysines can be acetylated
56 by histone acetyltransferases, and the number of acetylated residues correlates with
57 RNA transcription activity[15,16,19]. Among several H4 acetylation states[20-23], tetra-
58 acetylation at K5/K8/K12/K16 is particularly important, because this hyperacetylated
59 state is found in euchromatin regions where the nearby genes are transcriptionally most

60 active[24]. H4 acetylation at K5/K8/K12/K16 correlates with the expression of both the
61 RNAP II- and III-transcribed genes[15,16]. However, the contribution of each modification
62 state of each histone to the sequential steps of chromatin transcription is yet to be
63 quantified because of the difficulty in precise reconstitution of a chromatin template
64 with the epigenetic modification(s) of interest[25]. Using genetic code expansion and cell-
65 free protein synthesis, we synthesized histone H4 containing designed site-specific
66 acetylation(s) and reconstituted a H4-K5/K8/K12/K16-tetra-acetylated nucleosome[26,27].
67 Despite the suggested importance of tetra-acetylation at K5/K8/K12/K16, this
68 modification does not affect the crystal structure of the nucleosome core particle[27].
69 Therefore, the effect of histone H4 acetylation on the dynamics of the nucleosome core
70 needs to be analyzed.

71 Because the 5S rRNA gene can be chromatinized with a single nucleosome, it has
72 been used as a model gene in an *in vitro* chromatin transcription assay[28,29]. When whole
73 histones including the H4 tail are acetylated in a di-nucleosome chromatin template
74 containing a tandem of two 5S rRNA gene cassettes (*i.e.* X5S197-2[28]), 5S rRNA
75 transcription is activated *in vitro*[28]. However, it is difficult to monitor transcription in real
76 time because *in vitro* transcripts are usually detected by electrophoresis using
77 radioisotope-labeled UTP.

78 In this study, we developed a di-nucleosome tandem *Xenopus* 5S rRNA gene cassette
79 with a unique sequence derived from c-*fos*. Hybridization of nascent transcripts
80 containing this sequence with the corresponding antisense fluorescent probe enabled
81 real-time monitoring of transcript accumulation in a *Xenopus* oocyte nuclear extract by
82 fluorescence correlation spectroscopy (FCS). We reconstituted the di-nucleosome
83 chromatin template with non-acetylated or tetra-acetylated histone H4 and monitored

84 accumulation of 5S transcripts. Mathematical modeling allowed us to determine the
85 rates of chromatin remodeling from non-acetylated and H4-tetra-acetylated chromatin
86 templates. The methodology developed in this study can be used for quantitative
87 analysis of the contribution of epigenetic modification(s) to chromatin transcription.
88
89 **Results**
90 **Scheme of chromatin transcription, transcript detection, and modeling.** The
91 reconstituted RNAP III-driven chromatin transcription system used is shown in Fig. 1. For
92 analyzing the essential dynamics of chromatin transcription, we postulated four steps
93 on the basis of published data, each representing a chromatin state or reaction: (1)
94 chromatin accessibility, (2) chromatin remodeling, (3) priming before transcription, and
95 (4) 5S rRNA transcription.
96 Chromatin accessibility (1) for *trans*-acting factors can be evaluated by using
97 enzymes that act on DNA, such as micrococcal nuclease (MNase), DNase I, or
98 transposase[30]. Chromatin remodeling factors or histone chaperones, or both, may
99 access the chromatin template at different rates, depending on the presence or absence
100 of histone acetylation. Chromatin remodeling (2) includes remodeling or repositioning
101 (or both) of the nucleosome around the transcription start site. Chromatin remodeling
102 factors such as RSC (remodel the structure of chromatin), or histone chaperones such as
103 FACT (facilitates chromatin transcription), or both, allow access of *trans*-acting factors
104 (*e.g.*, transcriptional machinery) to DNA through relocation of the nucleosome at the
105 transcription start site, which is observed in both RNAP II and III-transcribed genes[31-33].
106 The extent to which a certain histone acetylation state facilitates chromatin remodeling
107 and nucleosome repositioning remains unclear[28,34,35]. Priming before transcription (3)

108 includes sequential assembly of the transcription preinitiation complex of general
109 transcription factors TFIIIA/TFIIIB/TFIIIC and RNAP III at the promoter[36-39]. Finally, 5S
110 rRNA is transcribed by RNAP III (4). During RNAP III-dependent transcription elongation,
111 the histone core is moving from a position on the DNA template ahead of RNAP III to a
112 position behind it[40-42]. Single nascent transcripts hybridizing with a fluorescent RNA
113 probe can be counted in real time by FCS microscopy. Using the above literature-based
114 chromatin transcription model, we aimed to establish a mathematical model to quantify
115 the contribution of a certain epigenetic modification state (tetra-acetylation of histone
116 H4 in this study) to chromatin transcription.
117
118 **Atomic force microscopy (AFM) imaging and micrococcal nuclease (MNase) digestion**
119 **of the H4-tetra-acetylated di-nucleosome.** We reconstituted a di-nucleosome in which
120 two copies of *Xenopus* somatic 5S rRNA gene were connected in tandem (Fig. 2A and
121 Supplementary Fig. 1)[25] and recombinant human histone H4 was either unmodified or
122 tetra-acetylated at K5/K8/K12/K16[26,27]. Site-specific acetylation of histone H4 at
123 K5/K8/K12/K16 was confirmed by Western blotting using specific monoclonal
124 antibodies (Fig. 2B). Histone octamers containing K5/K8/K12/K16-tetra-acetylated H4
125 (hereafter referred as 4Kac) or unmodified H4 together with bacterially expressed core
126 histones H2A, H2B, and H3[43] were assembled and purified. Using unmodified or 4Kac
127 histone octamers, 5S rRNA gene di-nucleosomes were reconstituted with either the
128 X5S197-2 template DNA (Fig. 2A, top; Supplementary Fig. 1A)[25,28] or the newly designed
129 X5S217F-2 template DNA (Fig. 2A, bottom; Supplementary Fig. 1B); X5S217F-2 had an
130 insertion of a 20-bp human c-*fos*-derived annealing sequence (which is absent in the

131 *Xenopus* genome) at the +115 position downstream of the 5S rRNA gene for specific
132 detection of 5S rRNA nascent transcripts.

133 Using AFM imaging, we found that the unmodified (Fig. 2C) and 4Kac (Fig. 2D)
134 X5S197-2 di-nucleosomes had similar dumbbell-shaped structures. DNA length between
135 the two nucleosome cores did not differ significantly between unmodified di-
136 nucleosomes (41 ± 12 nm; N = 50) and 4Kac di-nucleosomes (44 ± 10 nm; N = 50). We
137 next compared the biochemical accessibilities of micrococcal nuclease (MNase) to the
138 unmodified and 4Kac X5S197-2 di-nucleosomes (Fig. 2E). Toward both di-nucleosomes
139 (424 bp), MNase yielded approximately 145-bp DNA fragments that matched the length
140 of mono-nucleosomal DNA (145–147 bp). The sizes and amounts of this partially
141 digested DNA did not differ between unmodified and 4Kac di-nucleosomes (Fig. 2E),
142 suggesting that they had the same chromatin accessibility. Unmodified and 4Kac di-
143 nucleosomes reconstituted with X5S217F-2 template DNA (Fig. 2F) were used for real-
144 time chromatin transcription assay.

145

146 **Chromatin transcription and its real-time detection by FCS.** The X5S217F-2 di-
147 nucleosomes were transcribed in a *Xenopus* oocyte nuclear extract, which contains
148 RNAP III. An antisense RNA probe (20-nt-long Cy3-labeled 2'-*O*-methyl; 2OMe)[44] was
149 added to this system to bind to the complementary c-*fos*-derived annealing sequence in
150 the nascent 140-nt 5S rRNA transcript (Fig. 3A). Hybridization was assessed in real time
151 at high resolution as an increase in the diffusion time of the fluorescent antisense probe
152 detected by FCS[45-47] (Fig. 3B). When the engineered 5S rRNA is transcribed in the
153 reaction mixture, the diffusion time of the antisense probe, as determined from the
154 fluorescence autocorrelation function (FAF), was extended by sequence-dependent

155 hybridization, whereas 5S rRNA lacking the c-*fos* sequence did not extend the diffusion
156 time of the fluorescent antisense probe (Fig. 3C). For calibration of the transcription
157 level, different concentrations of the engineered 5S rRNA that had been transcribed by
158 T7 RNA polymerase were added to the reaction that contained all components except
159 the DNA template, and we conducted FCS measurements after 10-min incubation. The
160 relationship between the change in log RNA concentration and averaged diffusion time
161 of antisense probe in reaction mixture could be linearly approximated with an excellent
162 fit (correlation coefficient = 0.99; Fig. 3D), confirming that the concentration of nascent
163 transcripts can be quantified by measuring probe diffusion time.

164 By using a custom-made lid as a cover glass to prevent evaporation, we
165 obtained FAF using as little as 5 µl of the reaction mixtures, thus enabling us to measure
166 the concentrations of nascent transcripts *in vitro* in real time (Fig. 3E). As expected, no
167 RNA synthesis was observed for X5S197-2 naked DNA, which has no probe-annealing
168 sequence, whereas an increase in RNA concentration in a time-dependent manner was
169 observed for X5S217F-2 naked DNA (Fig. 3E). Transcription from the H4-tetra-acetylated
170 di-nucleosome was greater than that from the unmodified di-nucleosome, but both
171 were lower than that from the naked template (Fig. 3E). Hence, these results
172 demonstrate that site-specific acetylation of histone H4 activates chromatin
173 transcription *in vitro*.

174

175 **Mathematical modeling and analyses of chromatin transcription.** To quantify the
176 chromatin transcription kinetics, we constructed a simple mathematical model based on
177 steps (1)–(4) shown in Fig. 1. The definitions of the variables and parameters in our
178 mathematical model explained below are summarized in Supplementary Table 1. First,

179 the concentration of accessible chromatin is expressed by $\alpha_\xi C$, where ξ is the type of
180 chromatin template containing the c-*fos*-derived annealing sequence ('ξ' = '4Kac' for
181 H4-tetra-acetylated chromatin DNA or 'unmod' for unmodified chromatin DNA); C (=
182 300 nM, fixed) is the concentration of the template ('4Kac' and 'unmod'); and α_ξ is
183 accessibility of chromatin 'ξ'. Given $X_\xi(t)$ and $Y_\xi(t)$ are the concentrations of the
184 remodeled chromatin 'ξ' and primed chromatin 'ξ' at time t, respectively, the
185 concentration of chromatin 'ξ' to be remodeled is $\left(\alpha_\xi C - X_\xi - Y_\xi\right)$ (Fig. 4A). The
186 chromatin remodeling reaction is described as

187 $$\left(\alpha_\xi C - X_\xi - Y_\xi\right) \xrightarrow{k_\xi} X_\xi,$$

188 where k_ξ is the remodeling rate of chromatin 'ξ'. Thus, the priming reaction before
189 transcription is described as

190 $$X_\xi \xrightarrow{k_\mathrm{p}} Y_\xi,$$

191 where k_p is the priming rate of remodeled chromatin 'ξ'. Finally, 5S rRNA transcription
192 reaction is described as follows by assuming the Michaelis–Menten-type enzymatic
193 reaction

194 $$Y_\xi \xrightarrow{k_\mathrm{cat}, K_\mathrm{m}, C_\mathrm{RP}} Z_\xi,$$

195 where $Z_\xi(t)$ are the concentrations of the transcribed RNA produced from chromatin
196 'ξ' at time t; k_cat, K_m, and C_RP are the turnover number, the Michaelis–Menten constant,
197 and the concentration of RNAP III, respectively.

198 From the chemical reaction model, we have the following ordinary differential
199 equations:

200 $$\frac{\mathrm{d}X_\xi}{\mathrm{d}t} = k_\xi \left(\alpha_\xi C - X_\xi - Y_\xi\right) - k_\mathrm{p} X_\xi, \quad (1)$$

201 $$\frac{\mathrm{d}Y_\xi}{\mathrm{d}t} = k_\mathrm{p}\, X_\xi, \tag{2}$$

202 $$\frac{\mathrm{d}Z_\xi}{\mathrm{d}t} = \frac{k_\mathrm{cat} C_\mathrm{RP} Y_\xi}{K_\mathrm{m} + Y_\xi} \sim \frac{k_\mathrm{cat} C_\mathrm{RP}}{K_\mathrm{m}} Y_\xi, \tag{3}$$

203 where $K_\mathrm{m} \gg C > Y_\xi$ because K_m for eukaryotic RNA polymerase III is 7 to 83 μM[48]
204 and C in this study was 300 nM. By solving equations (1) – (3) under the initial condition
205 $X_\xi(0) = Y_\xi(0) = Z_\xi(0) = 0$, the kinetics of 5S rRNA transcription from the H4-tetra-
206 acetylated chromatin DNA and the unmodified chromatin DNA is obtained as

208 $$Z_\xi = \gamma \alpha_\xi \left[t - \left\{ \frac{k_p}{k_\xi (k_\xi - k_p)} e^{-k_\xi t} + \frac{k_\xi + k_p}{k_\xi k_p} - \frac{k_\xi}{k_p (k_\xi - k_p)} e^{-k_p t} \right\} \right], \tag{4}$$

207

209 where ξ is '4Kac' or 'unmod'; $\gamma = \frac{k_\mathrm{cat} C_\mathrm{RP}}{K_\mathrm{m}}$ is the transcription rate; the term $\gamma \alpha_\xi t$
210 means pure transcription without the need for chromatin remodeling or priming; the
211 term $-\left\{ \frac{k_p}{k_\xi (k_\xi - k_p)} e^{-k_\xi t} + \frac{k_\xi + k_p}{k_\xi k_p} - \frac{k_\xi}{k_p (k_\xi - k_p)} e^{-k_p t} \right\}$ indicates the pre-transcription
212 time delay caused by chromatin remodeling and priming (Fig. 4B).

213 By taking the limit of $k_\xi t \to \infty$, $k_p / k_\xi \to 0$, and $\alpha_\xi = 1$ in equation (4), the
214 kinetics of 5S rRNA transcription from the naked DNA containing the c-*fos*-derived
215 annealing sequence are

216 $$Z_\mathrm{naked} = \gamma \left[t - \frac{1 - e^{-k_\mathrm{p} t}}{k_\mathrm{p}} \right], \tag{5}$$

217 where Z_naked are the concentrations of the transcribed RNA produced from 'naked'
218 DNA at time *t* (Fig. 4C).

219 Using equations (4) and (5), we simulated dynamics of chromatin transcription
220 with different k_4Kac (Fig. 4D) and different α_4Kac (Fig. 4E). It was confirmed that the
221 chromatin remodeling rate k_ξ contributes to the time delay, not to the final slope of

222 the kinetics (Fig. 4D). On the other hand, the accessibility α_{ξ} contributes to the final
223 slope of the kinetics, not to the time delay (Fig. 4E).

224 Subsequently, we estimated the kinetic parameters of chromatin transcription by
225 fitting the experimental data to the mathematical model using the computing software
226 Mathematica 11.3 (Wolfram Research, Champaign, IL, USA). First, by fitting the
227 transcription data of the naked DNA to equation (5), the transcription rate γ and the
228 priming rate k_p were determined (Fig. 5A): γ ~ 0.046 nM min^{-1} and k_p ~ 0.13 min^{-1}. These
229 values were used to estimate the kinetics of transcription from all types of DNA
230 templates. Next, assuming $\alpha_{\mathrm{4Kac}} = \alpha_{\mathrm{unmod}} = 1$, fitting the 5S rRNA transcription data
231 of the H4-tetra-acetylated and unmodified chromatin DNA to equation (4) (Fig. 5B)
232 resulted in the chromatin remodeling rates k_{4Kac} ~ 0.12 min^{-1} and k_{unmod} ~ 0.039 min^{-1}.
233 Because all coefficients of determination, R^2, were sufficiently large (>0.93), the fitting
234 was considered to have been performed properly (Fig. 5A and 5B). This suggests that
235 the mathematical model constructed here can express the transcriptional dynamics. In
236 addition, to examine the adequacy of the assumption of $\alpha_{\mathrm{4Kac}} = \alpha_{\mathrm{unmod}} = 1$, we fitted
237 the data for $\alpha_{\mathrm{unmod}} = 0.8 - 1$ (Supplementary Fig. 2). Because the k_{unmod} and R^2
238 values did not change much even when α_{unmod} was changed, the simplest assumption
239 of $\alpha_{\mathrm{4Kac}} = \alpha_{\mathrm{unmod}} = 1$ was adopted on the basis of the results of MNase digestion
240 assays (Fig. 2E). Thus, the mathematical analysis shows the remodeling rate of H4-tetra-
241 acetylated chromatin DNA to be approximately 3-fold that of unmodified chromatin
242 DNA (k_{4Kac} / k_{unmod} ~ 3.1) (Fig. 5C).

243

244 **Discussion**

245 Although it has been known since the 1960s that acetylation of N-terminal tails of core
246 histones facilitates chromatin transcription[10,49], the contribution of each histone
247 modification state has not been quantified. In this study, we have developed a
248 methodology for such quantification by a fluorescence-based transcription tracking
249 method in a reconstituted system and mathematical modeling.

250 To understand the role of a particular epigenetic modification, a protein with
251 this modification has to be produced, for example by enzymatic modification[50], native
252 chemical ligation[51], or genetic code expansion[52,53]. To produce H4 histone with four sites
253 specifically acetylated, we combined genetic code expansion and cell-free protein
254 synthesis, but other methods may also be used. By comparing RNAP III-driven
255 transcription dynamics in unmodified and H4-tetra-acetylated di-nucleosomes
256 containing 5S rRNA gene cassettes, we established a platform to evaluate the rates of
257 transcription and chromatin remodeling. In this assay, the increase in chromatin
258 remodeling rate by H4 tetra-acetylation was approximately 3-fold (k_{4Kac} / k_{unmod} ~ 3.1).
259 This rate may be further increased by site-specific acetylation of other core histone
260 subunits[15]. Because the methodology developed here is versatile, the roles of other
261 histone PTMs (such as methylation and ubiquitination) can also be quantified. The
262 model may also be used for RNAP II-driven chromatin transcription, chromatin DNA
263 replication, and other aspects of DNA metabolism.

264 Real-time measurement of transcription in crude extracts is challenging
265 because the absolute amount of the reconstituted chromatin template is usually small,
266 which makes conventional measurements in a cuvette difficult. In this study, we
267 overcame this problem by using a fluorescent probe with high affinity and specificity,
268 and highly sensitive detection by FCS. Measurements of molecular diffusion by FCS

269 reduces the likelihood of obtaining false positives, which is a problem when solely
270 detecting a change in fluorescence. Furthermore, FCS, based on single molecule
271 counting, enables detection of RNA newly synthesized from a very small amount of
272 template. We found that minimization of the reaction volume (*e.g.*, less than 5 µl) and
273 extension of the measurement time (*e.g.*, more than 20 min) are technical bottlenecks
274 caused by evaporation of the reaction solution during the measurement. Considering
275 the femtoliter order of the FCS measurement region, much smaller volumes and longer
276 measurements can be achieved by integration with microfluidic device technologies. By
277 using the developed transcription tracking method in a reconstituted system, the effects
278 of chemical factors (*e.g.*, other PTMs, ions, pH) and physical factors (*e.g.*, temperature,
279 viscosity, congestion) on the dynamics of chromatin transcription can be investigated.
280 Considering the highly quantitative nature of FCS and the requirement for just a few-
281 microliter reaction volume, the present methodology may also be applicable to a living
282 cell[47].

283 Our mathematical model quantitatively describes the chromatin remodeling
284 step of eukaryotic chromatin transcription although it does not explicitly describe
285 nucleosome positioning and preinitiation complex formation. We obtained the
286 chromatin remodeling rates k_{4Kac} and k_{unmod} and confirmed the validity of data fitting, as
287 judged from their biochemically reasonable values. The remodeling rate of H4-tetra-
288 acetylated chromatin was approximately 3 times that of unmodified chromatin. This
289 finding is important for characterization of the effect of this modification: despite little
290 structural difference from unmodified chromatin, H4-tetra-acetylated chromatin
291 showed considerably more active dynamics of transcription. The effect of the difference

292 in chromatin remodeling rates observed in this study will be clearer when our
293 methodology is applied to living cells or other PTMs.

294 The constructed mathematical model [equation (4)] provides insights into
295 chromatin transcription. When focusing on a very short-term process ($k_\xi t \ll 1$), $Z_\xi \rightarrow$
296 $\frac{1}{6}\gamma\beta_\xi t^3$, where $\beta_\xi = \alpha_\xi k_\mathrm{p} k_\xi$ (min^{-2}); $\left(k_\mathrm{cat}\beta_\xi\right)^{\frac{1}{3}}$ (min^{-1}) is an apparent initial rate of
297 chromatin transcription. If very short-term transcription kinetics are quantitatively
298 measured, β_ξ or $\left(k_\mathrm{cat}\beta_\xi\right)^{\frac{1}{3}}$ can be used for classifying chromatin transcription in
299 various epigenetic modification states. When focusing on a long-term process ($k_\xi t \gg$
300 $1, k_\mathrm{p} t \gg 1$), $Z_\xi \rightarrow \gamma\alpha_\xi t$; thus, by measuring the slope of chromatin transcription,
301 chromatin accessibility can be determined more precisely, although in this study it was
302 assumed to be 1 on the basis of the results of MNase digestion assays.

303 In summary, we established an *in vitro* reconstitution system to quantify the
304 contribution of a certain epigenetic modification state to chromatin transcription
305 dynamics. As a model case, we compared the kinetics of chromatin remodeling and
306 transcription between unmodified and H4-tetra-acetylated chromatin templates.
307 Chromatin templates with certain PTMs, such as site-specific acetylation, can be used in
308 crude extracts in which the product molecules of interest can be counted in real time.
309 Therefore, our methodology will be applicable to a wide variety of chromatin-mediated
310 reactions for quantitative understanding of the importance of epigenetic modifications.
311

312 **Methods**

313 **Reconstitution of H4-acetylated histone octamers.** Core histones were prepared and
314 histone octamers were refolded essentially as described previously[54]. Briefly, the full-

315 length human histones H2A type 1-B/E, H2B type 1-J, and H3.1 were produced in *E. coli*
316 BL21 (DE3) and purified by Ni-Sepharose affinity chromatography. K5/K8/K12/K16-
317 acetylated histone H4 was produced in an *E. coli* cell-free protein synthesis system with
318 the expanded genetic code[26] as described in [27]. For refolding of histone octamers,
319 equimolar amounts of histones (*i.e.*, H2A, H2B, H3, and unmodified or tetra-acetylated
320 H4) were dissolved in 20 mM Tris-HCl buffer (pH 7.5) containing 6 M guanidine-HCl and
321 10 mM DTT, and dialyzed against 10 mM Tris-HCl buffer (pH 7.5) containing 2 M NaCl, 1
322 mM EDTA, and 5 mM 2-mercaptoethanol. The histone octamers were purified by size-
323 exclusion chromatography on a Superdex 200 column (GE Healthcare).
324
325 **Preparation of di-nucleosome DNA.** The 424-bp di-nucleosome DNA fragment X5S197-
326 2 composed of two tandem cassettes of the 197-bp *Xenopus borealis* somatic 5S rRNA
327 gene with an upstream sequence (Fig. 2A, top) was prepared as previously described[25].
328 To produce the 479-bp di-nucleosome DNA fragment (X5S217F-2; Fig. 2A, bottom), two
329 synthetic DNAs (250 bp and 229 bp) were purchased from Eurofins Genomics. The 250-
330 bp DNA was the first 5S rRNA gene cassette (–108 to +142), in which a *Pvu*II site (5'-
331 CAGCTG-3') was inserted at the 5' end and the c-*fos* antisense probe sequence (5'-
332 GCGGA GACAG ACCAA CTAGA-3') was inserted at the +115 position. The 229-bp DNA
333 was the second 5S rRNA gene cassette (–77 to +152), in which the c-*fos* antisense probe
334 sequence was inserted at the +115 position and the *Pvu*II site was inserted at the 3' end.
335 The two DNAs were ligated using a Gibson Assembly Master Mix (New England Biolabs)
336 and subcloned into the pWMD01 vector[55]. The di-nucleosome DNA with the modified
337 5S rRNA gene cassettes (X5S217F-2) was excised with *Pvu*II and purified by ion-exchange
338 chromatography on a TSK-gel DEAE-5PW column (Tosoh Corporation).

339

340 **Reconstitution of di-nucleosome chromatin templates.** Di-nucleosomes with or
341 without histone H4 acetylation were reconstituted by salt dialysis[25]. Briefly, purified
342 histone octamers were mixed with the X5S197-2 or X5S217F-2 fragment DNA in 10 mM
343 Tris-HCl buffer (pH 7.5) containing 2 M NaCl, 1 mM EDTA, and 1 mM 2-mercaptoethanol
344 (histone octamer: DNA = 0.9 : 1.0 w/w), and dialyzed at 4 °C for 16 h. Then, stepwise
345 dialysis was performed against buffers with decreasing NaCl concentrations. The
346 reconstituted di-nucleosomes were fractionated by centrifugation in 10%–25% sucrose
347 gradients at 36,000 rpm at 4 °C for 16 h in a Beckman SW41 rotor. Forty fractions were
348 collected using a Piston Gradient Fractionator (BioComp) and electrophoresed in 0.5×
349 TBE buffer at 8.5 V/cm in a 0.7% Seakem GTG agarose gel and visualized by ethidium
350 bromide staining. Di-nucleosomes from the 20th to 22nd fractions were pooled,
351 concentrated using an Amicon Ultra 0.5 ml 10K centrifugal filter, and dialyzed against 10
352 mM HEPES buffer (pH 7.5) containing 100 µM EDTA; their concentration was determined
353 from the optical density at a wavelength of 260 nm.

354

355 **Atomic force microscopy.** Di-nucleosomes (90 ng/µl) were fixed with 0.1%
356 glutaraldehyde for 16 h at 4 °C. Immediately before measurement, they were diluted to
357 0.45 ng/µl with 10 mM HEPES buffer (pH 7.5), placed onto APTES-treated mica[56] and left
358 for 10 min. Imaging was performed using a high-speed AFM system (Nano Live Vision,
359 RIBM, Tsukuba, Japan) with a carbon nanofiber cantilever (BL-AC10FS, Olympus) at a
360 spring constant of 0.1 N/m in solution phase at 27 °C. Images of a 500 × 375-nm area
361 were obtained at 2 s/frame at a resolution of 192 × 144 pixels. DNA length between two

362 nucleosome core particles was traced manually in the images and quantified using
363 ImageJ software (version 1.45s).
364
365 **Micrococcal nuclease digestion.** DNA of di-nucleosome (100 ng) containing either tetra-
366 acetylated or unmodified histone H4 was digested for 5 min at 22 °C with MNase (0.125
367 to 2.0 units; Takara, cat. #2910A) in 5.5 mM Tris-HCl buffer (pH 7.6) containing 500 µM
368 $CaCl_2$ and 50 µg/ml BSA. Digestion was terminated by addition of 20 mM EDTA and 0.5%
369 (w/v) SDS containing 2 µg of proteinase K (Roche, cat. #3115887). DNA fragments were
370 extracted with phenol/chloroform and analyzed by electrophoresis in a non-denaturing
371 10% polyacrylamide gel.
372
373 **Transcription *in vitro* and transcript detection by fluorescence correlation**
374 **spectroscopy.** Transcription was performed essentially as described[57]. Each reaction
375 mixture (10 µl) contained purified di-nucleosome or naked DNA template (1 µg) , 0.9 µl
376 of a *Xenopus* oocyte nuclear extract, 9.5 mM HEPES (pH 7.4), 100 mM NaCl, 48 mM KCl,
377 6.7 mM $MgCl_2$, 3.6 mM DTT, 90 µM EDTA, 4.5% (v/v) glycerol, 0.9% (w/v)
378 polyvinylpyrrolidone, 0.06% (w/v) BSA, 500 µM NTPs, 1 µM trichostatin A, 5 units of
379 RNase inhibitor (Toyobo, cat. #SIN-201), and 20 nM c-*fos* antisense probe. The c-*fos*
380 probe was synthesized with a 2′ O-Me RNA backbone, which was labeled with Cy3 at its
381 3′ end. FCS was conducted on a confocal laser-scanning fluorescence microscope (TCS
382 SP8, Leica) equipped with a single molecule detection unit (PicoQuant) at 23 °C. The
383 reaction mixture (5 µl) was covered with a stainless-steel cylinder (inner diameter, 6.2
384 mm; length, 5 mm), one end of which was covered with a cover glass. Cy3 fluorescence
385 was excited with a green laser (532 nm, Leica), and emitted photons were captured

through an objective lens (63×, HC PL APO CS2 1.20 N.A. water, Leica) with a 570DF30 emission filter (Omega). Each 30-s fluorescence fluctuation measurement was performed with an avalanche photodiode (PicoQuant). Total recording time was about 20 min. Autocorrelation was calculated with the SymPhoTime software (PicoQuant). The obtained fluorescence autocorrelation between 0.01 and 813 ms was approximated with SymPhoTime using the autocorrelation function [equation (6)] with one component:

$$\mathrm{G}(\tau) - 1 = \frac{1}{N} \times \left(\frac{1}{1+\tau/\tau_1}\right)\left(\frac{1}{1+(1/\kappa)^2(\tau/\tau_1)}\right)^{\frac{1}{2}} \quad (6)$$

where N is the number of fluorescent dyes in the confocal volume, τ_1 is the diffusion time, and κ is a structure parameter (10–15 in this experiment).

Author contributions

M.W., K.O., M.T., and T.U. designed the experiments, interpreted the results, and wrote the manuscript. M.W., K.U., and T.U. performed the biochemical analysis. K.O. and T.F. performed the biophysical analysis. M.T. performed the mathematical analysis. All authors commented on the manuscript.

Acknowledgments

We thank Hiroki R. Ueda (the University of Tokyo) for encouragement, Toshiaki Higo for sample preparation, and Yuki Saito for clerical assistance. This work was supported by grants from the PRESTO program of the Japan Science and Technology Agency (JST), and in part by Grants-in-Aid for Scientific Research on Innovative Areas to K.O. (No. 15H05931) and K.U. (No. 15H01345), a Grant-in-Aid for Challenging Research (Exploratory) to M.T. (No. 18K19834), and Grants-in-Aid for Scientific Research (B) to

M.T. (No. 17H01813) and T.U. (No. 16H05089) from the Japan Society for the Promotion of Science (JSPS).

References

1 Roeder, R. G. & Rutter, W. J. Multiple forms of DNA-dependent RNA polymerase in eukaryotic organisms. *Nature* **224**, 234-237 (1969).

2 Dignam, J. D., Lebovitz, R. M. & Roeder, R. G. Accurate transcription initiation by RNA polymerase II in a soluble extract from isolated mammalian nuclei. *Nucleic acids research* **11**, 1475-1489 (1983).

3 Keener, J., Josaitis, C. A., Dodd, J. A. & Nomura, M. Reconstitution of yeast RNA polymerase I transcription in vitro from purified components. TATA-binding protein is not required for basal transcription. *The Journal of biological chemistry* **273**, 33795-33802 (1998).

4 Vannini, A. & Cramer, P. Conservation between the RNA polymerase I, II, and III transcription initiation machineries. *Molecular cell* **45**, 439-446, doi:10.1016/j.molcel.2012.01.023 (2012).

5 Paranjape, S. M., Kamakaka, R. T. & Kadonaga, J. T. Role of chromatin structure in the regulation of transcription by RNA polymerase II. *Annual review of biochemistry* **63**, 265-297 (1994).

6 Felsenfeld, G. Chromatin as an essential part of the transcriptional mechanism. *Nature* **355**, 219, doi:10.1038/355219a0 (1992).

7 Luger, K., Mader, A. W., Richmond, R. K., Sargent, D. F. & Richmond, T. J. Crystal structure of the nucleosome core particle at 2.8 A resolution. *Nature* **389**, 251-260, doi:10.1038/38444 (1997).

8 Kornberg, R. D. & Lorch, Y. L. Twenty-five years of the nucleosome, fundamental particle of the eukaryote chromosome. *Cell* **98**, 285-294, doi:10.1016/S0092-8674(00)81958-3 (1999).

9 Peterson, C. L. & Laniel, M.-A. Histones and histone modifications. *Current Biology* **14**, R546-R551, doi:10.1016/j.cub.2004.07.007 (2004).

10 Allfrey, V. G., Faulkner, R. & Mirsky, A. E. Acetylation and Methylation of Histones and Their Possible Role in the Regulation of RNA Synthesis. *Proceedings of the National Academy of Sciences of the United States of America* **51**, 786-794 (1964).

11 Lee, D. Y., Hayes, J. J., Pruss, D. & Wolffe, A. P. A positive role for histone acetylation in transcription factor access to nucleosomal DNA. *Cell* **72**, 73-84 (1993).

12 Hirschler-Laszkiewicz, I. *et al.* The role of acetylation in rDNA transcription. *Nucleic acids research* **29**, 4114-4124 (2001).

13 Eberharter, A. & Becker, P. B. Histone acetylation: a switch between repressive and permissive chromatin. *Second in review series on chromatin dynamics* **3**, 224-229, doi:10.1093/embo-reports/kvf053 (2002).

14 Grummt, I. & Pikaard, C. S. Epigenetic silencing of RNA polymerase I transcription. *Nature reviews. Molecular cell biology* **4**, 641-649, doi:10.1038/nrm1171 (2003).

15 Barski, A. *et al.* Pol II and its associated epigenetic marks are present at Pol III–transcribed noncoding RNA genes. *Nature structural & molecular biology* **17**, 629 (2010).

16 White, R. J. Transcription by RNA polymerase III: more complex than we thought. *Nature reviews. Genetics* **12**, 459-463, doi:10.1038/nrg3001 (2011).

17 Wolffe, A. P. Nucleosome positioning and modification: chromatin structures that potentiate transcription. *Trends in biochemical sciences* **19**, 240-244 (1994).

18 Jiang, C. & Pugh, B. F. Nucleosome positioning and gene regulation: advances through genomics. *Nature Reviews Genetics* **10**, 161, doi:10.1038/nrg2522 (2009).

19 Turner, B. M. Histone acetylation and control of gene expression. *Journal of cell science* **99**, 13-20 (1991).

20 Zhang, K. *et al.* Histone Acetylation and Deacetylation. *Identification of Acetylation and Methylation Sites of HeLa Histone H4 by Mass Spectrometry* **1**, 500-508, doi:10.1074/mcp.M200031-MCP200 (2002).

21 Smith, C. M. *et al.* Mass spectrometric quantification of acetylation at specific lysines within the amino-terminal tail of histone H4. *Analytical biochemistry* **316**, 23-33, doi:10.1016/S0003-2697(03)00032-0 (2003).

22 Wang, C. I. *et al.* ChIP-mass spectrometry captures protein interactions and modified histones associated with dosage compensation in Drosophila. *Nature structural & molecular biology* **20**, 202-209, doi:10.1038/nsmb.2477 (2013).

23 Henry, R. A. *et al.* Quantitative measurement of histone tail acetylation reveals stage-specific regulation and response to environmental changes during Drosophila development. *Biochemistry-Us* **55**, 1663-1672, doi:10.1021/acs.biochem.5b01070 (2016).

24 Grunstein, M. Histone acetylation in chromatin structure and transcription. *Nature* **389**, 349, doi:10.1038/38664 (1997).

25 Ura, K., Hayes, J. J. & Wolffe, A. P. A positive role for nucleosome mobility in the transcriptional activity of chromatin templates: restriction by linker histones. *The EMBO journal* **14**, 3752-3765 (1995).

26 Mukai, T. *et al.* Genetic-code evolution for protein synthesis with non-natural amino acids. *Biochemical and biophysical research communications* **411**, 757-761, doi:10.1016/J.Bbrc.2011.07.020 (2011).

27 Wakamori, M. *et al.* Intra- and inter-nucleosomal interactions of the histone H4 tail revealed with a human nucleosome core particle with genetically-incorporated H4 tetra-acetylation. *Scientific reports* **5**, 17204, doi:10.1038/srep17204 (2015).

28 Ura, K., Kurumizaka, H., Dimitrov, S., Almouzni, G. & Wolffe, A. P. Histone acetylation: influence on transcription, nucleosome mobility and positioning, and linker histone-dependent transcriptional repression. *The EMBO journal* **16**, 2096-2107, doi:10.1093/emboj/16.8.2096 (1997).

29 Tse, C., Sera, T., Wolffe, A. P. & Hansen, J. C. Disruption of higher-order folding by core histone acetylation dramatically enhances transcription of nucleosomal arrays by RNA polymerase III. *Mol Cell Biol* **18**, 4629-4638 (1998).

30 Tsompana, M. & Buck, M. J. Chromatin accessibility: a window into the genome. *Epigenetics & chromatin* **7**, 33, doi:10.1186/1756-8935-7-33 (2014).

31 Birch, J. L. *et al.* FACT facilitates chromatin transcription by RNA polymerases I and III. *The EMBO journal* **28**, 854-865, doi:10.1038/emboj.2009.33 (2009).

32 Helbo, A. S., Lay, F. D., Jones, P. A., Liang, G. & Gronbaek, K. Nucleosome Positioning and NDR Structure at RNA Polymerase III Promoters. *Scientific reports* **7**, 41947, doi:10.1038/srep41947 (2017).

33 Parnell, T. J., Huff, J. T. & Cairns, B. R. RSC regulates nucleosome positioning at Pol II genes and density at Pol III genes. *The EMBO journal* **27**, 100-110, doi:10.1038/sj.emboj.7601946 (2008).

34 Bresnick, E. H., John, S. & Hager, G. L. Histone hyperacetylation does not alter the positioning or stability of phased nucleosomes on the mouse mammary tumor virus long terminal repeat. *Biochemistry-Us* **30**, 3490-3497 (1991).

35 Eberharter, A. & Becker, P. B. Histone acetylation: a switch between repressive and permissive chromatin. Second in review series on chromatin dynamics. *EMBO reports* **3**, 224-229, doi:10.1093/embo-reports/kvf053 (2002).

36 Dieci, G., Fiorino, G., Castelnuovo, M., Teichmann, M. & Pagano, A. The expanding RNA polymerase III transcriptome. *Trends in Genetics* **23**, 614-622, doi:10.1016/j.tig.2007.09.001 (2007).

37 Orioli, A., Pascali, C., Pagano, A., Teichmann, M. & Dieci, G. RNA polymerase III transcription control elements: Themes and variations. *Gene* **493**, 185-194, doi:10.1016/j.gene.2011.06.015 (2012).

38 Arimbasseri, A. G., Rijal, K. & Maraia, R. J. Comparative overview of RNA polymerase II and III transcription cycles, with focus on RNA polymerase III termination and reinitiation. *Transcription* **5**, e27639, doi:10.4161/trns.27369 (2014).

39 Leśniewska, E. & Boguta, M. Novel layers of RNA polymerase III control affecting tRNA gene transcription in eukaryotes. *Open biology* **7**, 170001, doi:10.1098/rsob.170001 (2017).

40 Clark, D. J. & Felsenfeld, G. A nucleosome core is transferred out of the path of a transcribing polymerase. *Cell* **71**, 11-22 (1992).

41 Studitsky, V. M., Kassavetis, G. A., Geiduschek, E. P. & Felsenfeld, G. Mechanism of Transcription Through the Nucleosome by Eukaryotic RNA Polymerase. *Science* **278**, 1960-1963, doi:10.1126/science.278.5345.1960 (1997).

42 Workman, J. L. Nucleosome displacement in transcription. *Genes & development* **20**, 2009-2017, doi:10.1101/gad.1435706 (2006).

43 Dyer, P. N. *et al.* Reconstitution of nucleosome core particles from recombinant histones and DNA. *Methods in enzymology* **375**, 23-44 (2004).

44 Okabe, K. *et al.* Real time monitoring of endogenous cytoplasmic mRNA using linear antisense 2′ -O-methyl RNA probes in living cells. *Nucleic acids research* **39**, e20-e20, doi:10.1093/nar/gkq1196 (2011).

45 Kettling, U., Koltermann, A., Schwille, P. & Eigen, M. Real-time enzyme kinetics monitored by dual-color fluorescence cross-correlation spectroscopy. *Proceedings of the National Academy of Sciences* **95**, 1416-1420, doi:10.1073/pnas.95.4.1416 (1998).

46 Medina, M. Á. & Schwille, P. Fluorescence correlation spectroscopy for the detection and study of single molecules in biology. *Bioessays* **24**, 758-764, doi:doi:10.1002/bies.10118 (2002).

47 Zhang, J., Okabe, K., Tani, T. & Funatsu, T. Dynamic association-dissociation and harboring of endogenous mRNAs in stress granules. *Journal of cell science* **124**, 4087-4095, doi:10.1242/jcs.090951 (2011).

48 Szafranski, P. & Smagowicz, W. J. Relative affinities of nucleotide substrates for the yeast tRNA gene transcription complex. *Zeitschrift fur Naturforschung. C, Journal of biosciences* **47**, 320-321 (1992).

49 Verdin, E. & Ott, M. 50 years of protein acetylation: from gene regulation to epigenetics, metabolism and beyond. *Nature reviews. Molecular cell biology* **16**, 258-264, doi:10.1038/nrm3931 (2015).

50 Mishima, Y. *et al.* Hinge and chromoshadow of HP1alpha participate in recognition of K9 methylated histone H3 in nucleosomes. *Journal of molecular biology* **425**, 54-70, doi:10.1016/j.jmb.2012.10.018 (2013).

51 Fierz, B. & Muir, T. W. Chromatin as an expansive canvas for chemical biology. *Nat Chem Biol* **8**, 417-427, doi:10.1038/nchembio.938 (2012).

52 Yanagisawa, T., Umehara, T., Sakamoto, K. & Yokoyama, S. Expanded genetic code technologies for incorporating modified lysine at multiple sites. *Chembiochem : a European journal of chemical biology* **15**, 2181-2187, doi:10.1002/cbic.201402266 (2014).

53 Chin, J. W. Expanding and reprogramming the genetic code. *Nature* **550**, 53-60, doi:10.1038/nature24031 (2017).

54 Tanaka, Y. *et al.* Expression and purification of recombinant human histones. *Methods* **33**, 3-11, doi:10.1016/j.ymeth.2003.10.024 (2004).

55 Wakamori, M., Umehara, T. & Yokoyama, S. A tandem insertion vector for large-scale preparation of nucleosomal DNA. *Analytical biochemistry* **423**, 184-186, doi:10.1016/j.ab.2012.01.010 (2012).

56 Wang, H. *et al.* Glutaraldehyde Modified Mica: A New Surface for Atomic Force Microscopy of Chromatin. *Biophysical journal* **83**, 3619-3625, doi:10.1016/S0006-3495(02)75362-9 (2002).

57 Birkenmeier, E. H., Brown, D. D. & Jordan, E. A nuclear extract of Xenopus laevis oocytes that accurately transcribes 5S RNA genes. *Cell* **15**, 1077-1086 (1978).

567 **Figure Legends**

568 **Figure 1.** Schematic diagram of 5S rRNA chromatin transcription and its real-time
569 detection.

570

571 **Figure 2.** Reconstitution of H4-tetra-acetylated di-nucleosomes for chromatin
572 transcription. (A) Scheme of di-nucleosome rRNA gene cassettes. Internal control
573 regions (box A; IE, intermediate element; box C) of the 5S rRNA gene are indicated. The
574 X5S197-2 construct[28] (top) was modified by introducing a c-*fos* probe sequence (bottom)
575 for fluorescence correlation spectroscopy measurements. (B) Western blotting of
576 unmodified and site-specifically tetra-acetylated histone H4 proteins. Kac, acetylated
577 lysine. (C, D) Atomic force microscopy images of 5S rRNA di-nucleosomes reconstituted
578 with unmodified histone H4 (C) or K5/K8/K12/K16-acetylated H4 (D). (E) Di-nucleosome
579 digestion with micrococcal nuclease (MNase). Lanes 1, 3, 5, 7 and 9, di-nucleosomes
580 with unmodified H4; lanes 2, 4, 6, 8 and 10, di-nucleosomes with K5/K8/K12/K16-
581 acetylated H4. Lanes 1 and 2, di-nucleosomes were incubated in MNase reaction buffer
582 in the absence of MNase. Units of MNase (Takara, cat. #2910A) per microgram DNA:
583 lanes 3 and 4, 2.5; lanes 5 and 6, 5.0; lanes 7 and 8, 10, lanes 9 and 10, 20. (F) Agarose
584 gel electrophoreses of di-nucleosomes constructed with c-*fos*-derived annealing
585 sequence DNA. Lane M, DNA ladder marker (NEB, cat. N3232S); lane 1, di-nucleosome
586 reconstituted with unmodified H4; lane 2, di-nucleosome reconstituted with
587 K5/K8/K12/K16-tetra-acetylated H4.

588

589 **Figure 3.** Real-time detection of chromatin transcription. (A) Scheme of a Cy3-labeled
590 antisense 2'-*O*-methyl RNA (2OMe-RNA) probe and its hybridization with mRNA. (B)

591 Scheme of the setup of fluorescence correlation spectroscopy (FCS) for monitoring
592 mRNA synthesis. Changes in diffusion of the antisense probe upon hybridization with
593 transcripts in the confocal volume were detected by an avalanche photodiode (APD) at
594 the single-molecule level. (C) Fluorescence autocorrelation functions [FAF, G(τ)] in
595 reaction solutions. FAF of the antisense probe with mRNA showed longer correlation
596 time than that without mRNA or that of a control probe with mRNA. (Inset) averaged
597 diffusion time of antisense probes. (D) Calibration of the averaged diffusion time of the
598 antisense 5S/c-*fos* RNA probe molecules as a function of their concentration. In (C) and
599 (D), RNA was transcribed by T7 RNA polymerase from two tandem copies of the 5S rRNA
600 gene (Fig. 2A) and added to a *Xenopus* oocyte nuclear extract without template DNA;
601 diffusion time was measured by FCS. Mean ± standard deviation (*N* = 3). (E) Real-time
602 detection of nascent 5S rRNA transcripts. Template DNAs used are shown in: gray, naked
603 5S rRNA gene without c-*fos* sequence; black, naked 5S rRNA gene containing the c-*fos*-
604 derived annealing sequence; red, H4-tetra-acetylated di-nucleosome 5S rRNA gene
605 containing c-*fos* sequence; and blue, non-acetylated di-nucleosome 5S rRNA gene
606 containing c-*fos* sequence.
607
608 **Figure 4.** Mathematical model of chromatin transcription. (A) Explanation of modeling
609 of chromatin transcription. Variables are defined in Supplementary Table 1. (B, C)
610 Explanation of the obtained equations. (B) Transcription from chromatin [equation (4)].
611 (C) Transcription from naked DNA [equation (5)]. (D, E) Numerical simulation of
612 chromatin transcription with different $k_{4\mathrm{Kac}}$ (D) and different $\alpha_{4\mathrm{Kac}}$ (E). $\gamma = 0.01$
613 nM min^{-1} and $k_p = 1/15 \approx 0.0667$ min^{-1} are fixed. Z_ξ is the concentration of
614 transcribed RNA, where ξ is '4Kac' or 'naked'. For '4Kac', equation (4) is used, where

615 $k_{4\mathrm{Kac}}$ is changed with $\alpha_{4\mathrm{Kac}} = \alpha_{\mathrm{naked}} = 1$ fixed (D) or $\alpha_{4\mathrm{Kac}}$ is changed with

616 $\alpha_{\mathrm{naked}} = 1$ and $k_{4\mathrm{Kac}} = 0.1$ min^{-1} fixed (E). For 'naked', equation (5) is used.

617

618 **Figure 5.** Results of fitting to the mathematical model. (A) Determination of γ and k_{p}.

619 First, the γ value was determined by fitting the linear region (12–17 min) of the

620 experimental data for the naked DNA (+ c-*fos*) to the mathematical model $Z_{\mathrm{naked}} =$

621 $\gamma t + z_1$, where z_1 is the intercept; this equation is the long-term limit of equation (5).

622 As a result, γ = 0.046 ± 0.003 nM min^{-1} ('fitting value' ± 'fitting error') (z_1 = –0.29 ± 0.04

623 nM; coefficient of determination R^2 = 0.998). Then, using the obtained γ, the k_{p} value

624 was determined by fitting the whole region (0–17 min) of the data to the mathematical

625 model $Z_{\mathrm{naked}} = \gamma\left[\, t \, - \left(1 - e^{-k_{\mathrm{p}} t}\right)/k_{\mathrm{p}} \,\right] + z_2$, where z_2 is the intercept introduced

626 for resolving experimental error at the initial stage [equation (5)]. As a result, k_{p} = 0.13

627 ± 0.006 min^{-1} (z_2 = –0.010 ± 0.006 nM; R^2 = 0.993). (B) Fitting results for each condition.

628 Z_{ξ} is the concentration of transcribed RNA, where ξ is '4Kac', 'unmod', or 'naked'

629 [equations (4) and (5)]. γ = 0.046 nM min^{-1} and k_{p} = 0.13 min^{-1}, which were obtained in

630 (A), were used for fitting. (C) Schematic illustration of acceleration of chromatin

631 transcription by histone H4 acetylation.

Figure 1

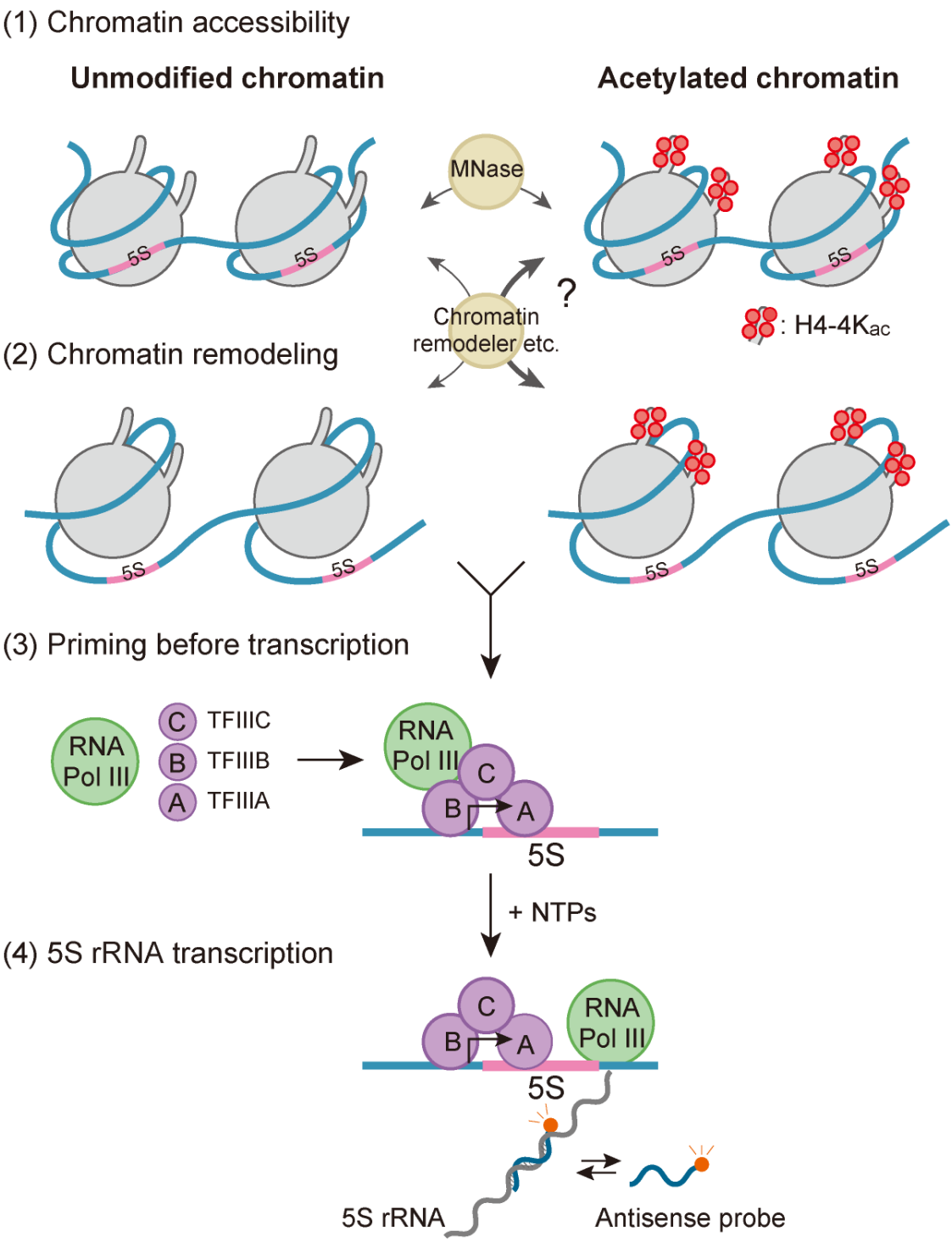
(1) Chromatin accessibility
Unmodified chromatin
Acetylated chromatin
MNase
5S
Chromatin remodeler etc.
?
: H4-4Kac
(2) Chromatin remodeling
(3) Priming before transcription
RNA Pol III
C TFIIIC
B TFIIIB
A TFIIIA
+ NTPs
(4) 5S rRNA transcription
5S rRNA
Antisense probe

Figure 2

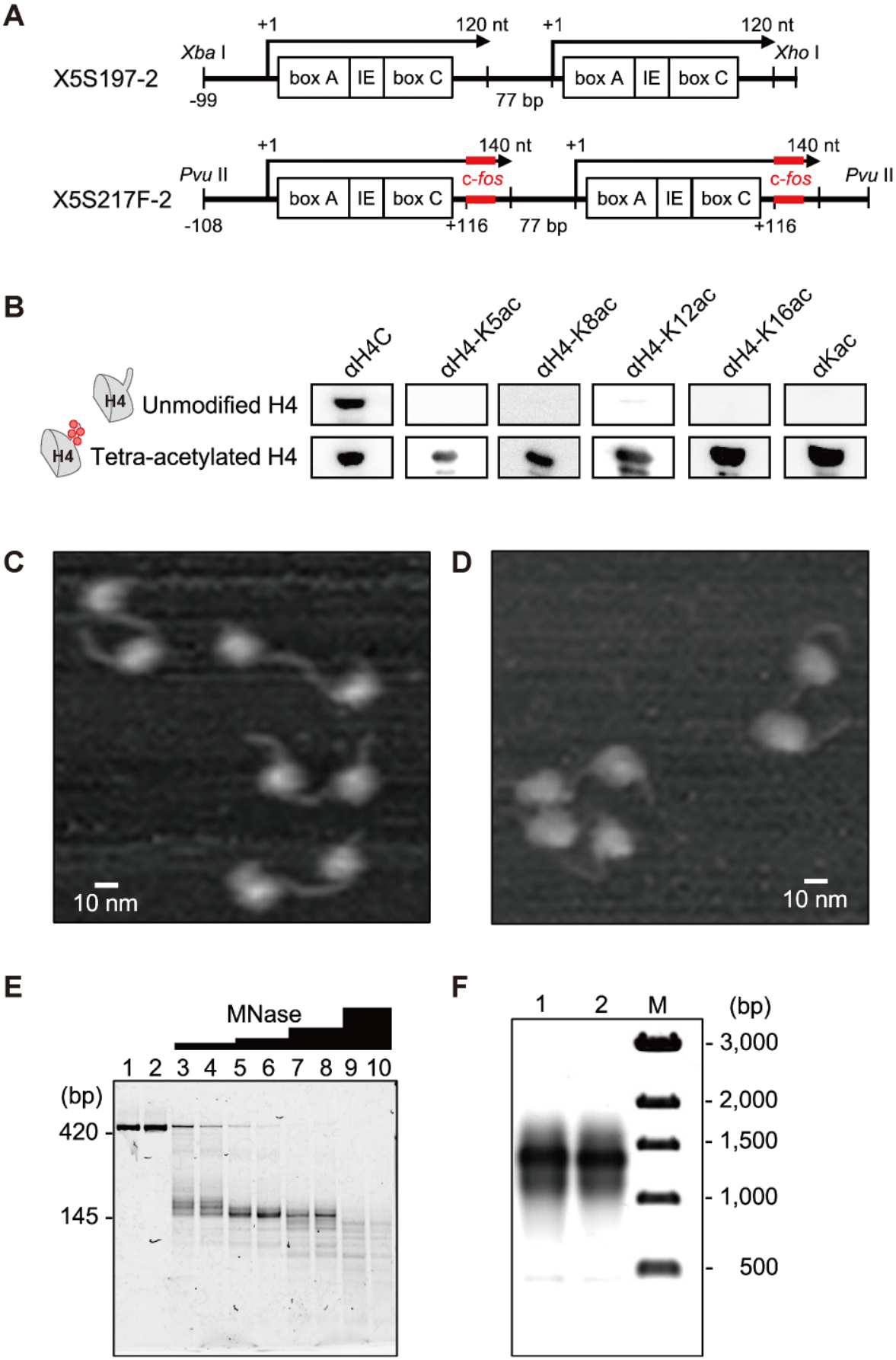
A
X5S197-2
Xba I
+1
120 nt
box A
IE
box C
-99
77 bp
Xho I
X5S217F-2
Pvu II
140 nt
c-fos
-108
+116
B
αH4C
αH4-K5ac
αH4-K8ac
αH4-K12ac
αH4-K16ac
αKac
Unmodified H4
Tetra-acetylated H4
C
10 nm
D
E
MNase
1 2 3 4 5 6 7 8 9 10
(bp)
420
145
F
1 2 M
(bp)
3,000
2,000
1,500
1,000
500

Figure 3

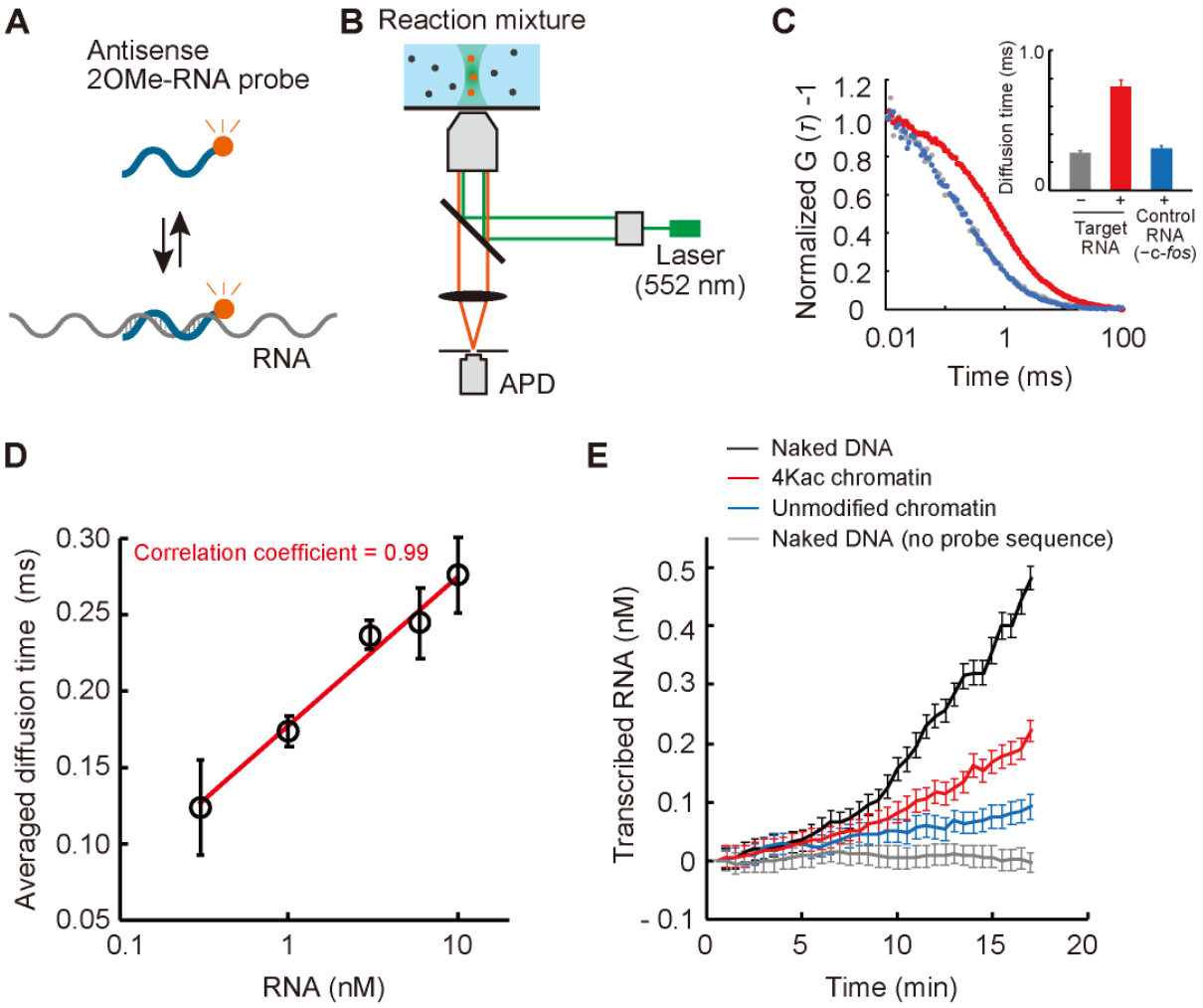
A
Antisense
2OMe-RNA probe
RNA
B Reaction mixture
Laser
(552 nm)
APD
C
Normalized G (τ) -1
1.2
1.0
0.8
0.6
0.4
0.2
0
0.01
1
100
Time (ms)
Diffusion time (ms)
1.0
0
Target RNA
Control RNA (−c-fos)
D
Correlation coefficient = 0.99
Averaged diffusion time (ms)
0.30
0.25
0.20
0.15
0.10
0.05
0.1
1
10
RNA (nM)
E
Naked DNA
4Kac chromatin
Unmodified chromatin
Naked DNA (no probe sequence)
Transcribed RNA (nM)
0.5
0.4
0.3
0.2
0.1
0
- 0.1
0
5
10
15
20
Time (min)

Figure 4

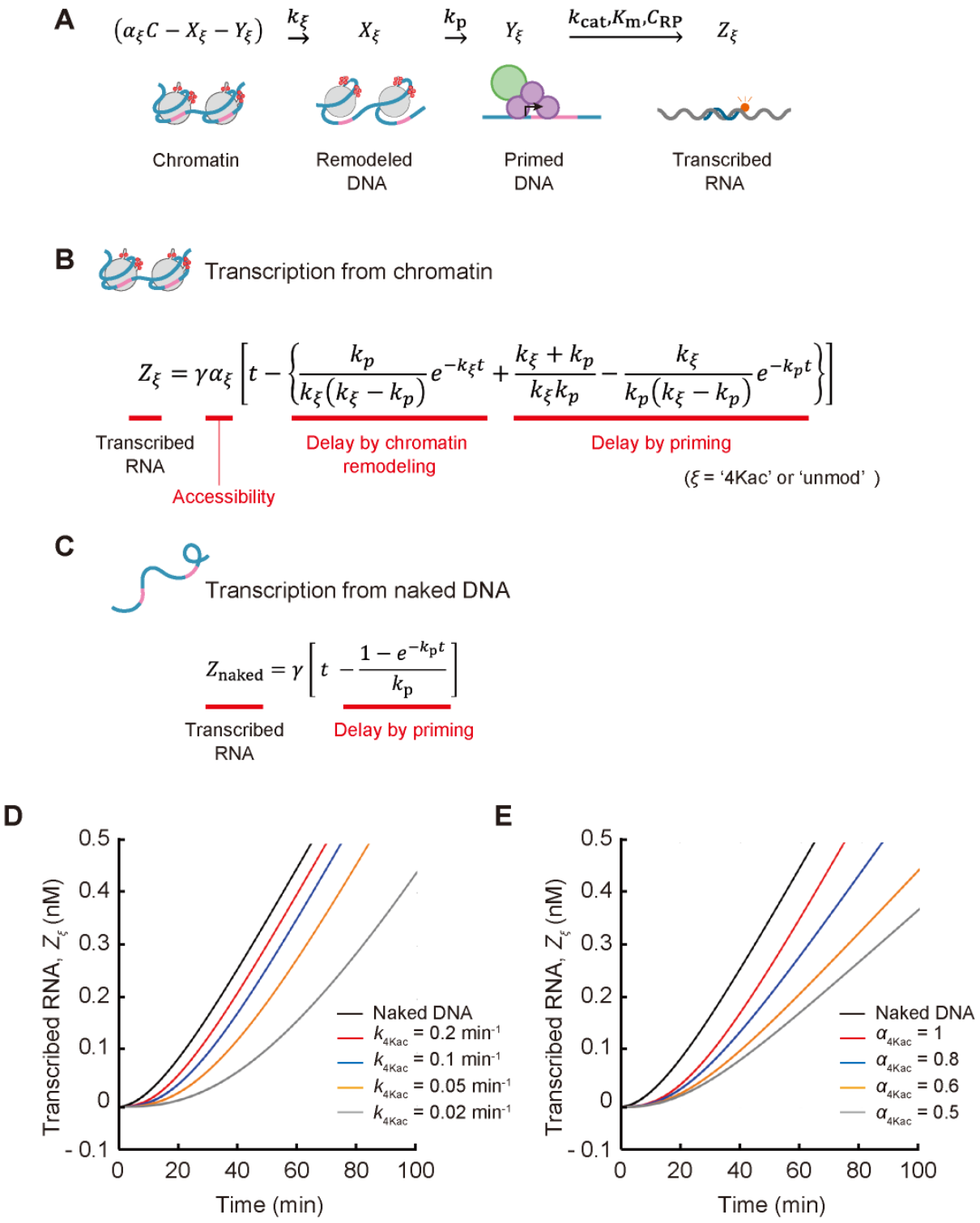
A
$(\alpha_\xi C - X_\xi - Y_\xi) \xrightarrow{k_\xi} X_\xi \xrightarrow{k_p} Y_\xi \xrightarrow{k_{cat}, K_m, C_{RP}} Z_\xi$
Chromatin
Remodeled DNA
Primed DNA
Transcribed RNA
B
Transcription from chromatin
$Z_\xi = \gamma\alpha_\xi \left[t - \left\{ \frac{k_p}{k_\xi(k_\xi - k_p)} e^{-k_\xi t} + \frac{k_\xi + k_p}{k_\xi k_p} - \frac{k_\xi}{k_p(k_\xi - k_p)} e^{-k_p t} \right\} \right]$
Transcribed RNA
Accessibility
Delay by chromatin remodeling
Delay by priming
(ξ = '4Kac' or 'unmod')
C
Transcription from naked DNA
$Z_{naked} = \gamma \left[t - \frac{1 - e^{-k_p t}}{k_p} \right]$
Transcribed RNA
Delay by priming
D
Transcribed RNA, Z_ξ (nM)
Time (min)
Naked DNA
k_{4Kac} = 0.2 min^{-1}
k_{4Kac} = 0.1 min^{-1}
k_{4Kac} = 0.05 min^{-1}
k_{4Kac} = 0.02 min^{-1}
E
Transcribed RNA, Z_ξ (nM)
Time (min)
Naked DNA
α_{4Kac} = 1
α_{4Kac} = 0.8
α_{4Kac} = 0.6
α_{4Kac} = 0.5

Figure 5

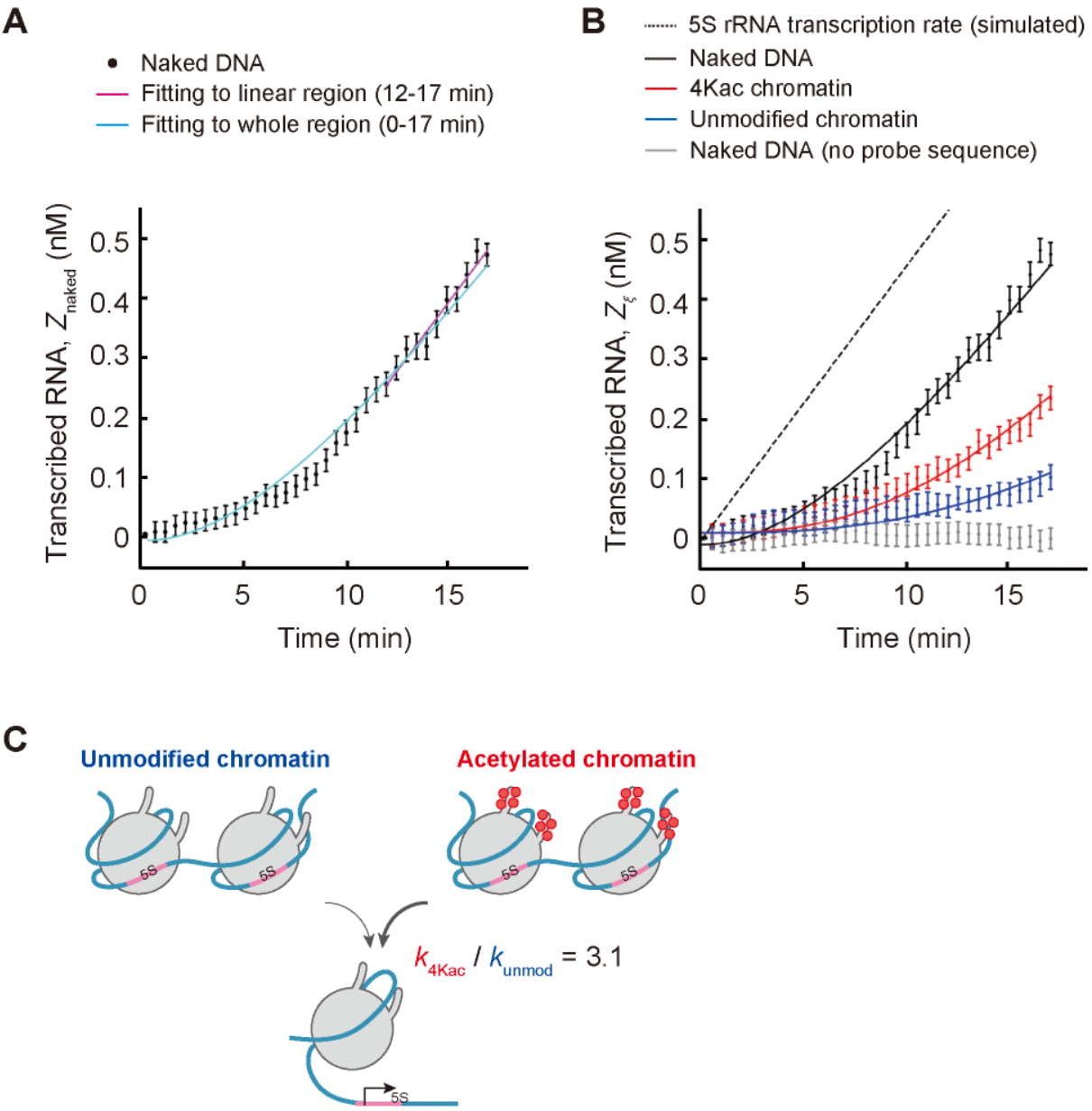
A
Naked DNA
Fitting to linear region (12-17 min)
Fitting to whole region (0-17 min)
Transcribed RNA, Z_{naked} (nM)
0.5
0.4
0.3
0.2
0.1
0
0
5
10
15
Time (min)
B
5S rRNA transcription rate (simulated)
Naked DNA
4Kac chromatin
Unmodified chromatin
Naked DNA (no probe sequence)
Transcribed RNA, Z_{ξ} (nM)
0.5
0.4
0.3
0.2
0.1
0
0
5
10
15
Time (min)
C
Unmodified chromatin
Acetylated chromatin
5S
5S
5S
5S
$k_{4Kac} / k_{unmod} = 3.1$
5S